

# Planning Optimal Trajectories for Mobile Manipulators under End-effector Trajectory Continuity Constraint

Quang-Nam Nguyen<sup>1</sup> and Quang-Cuong Pham<sup>1,2</sup>

**Abstract**—Mobile manipulators have been employed in many applications which are usually performed by multiple fixed-base robots or a large-size system, thanks to the mobility of the mobile base. However, the mobile base also brings redundancies to the system, which makes trajectory planning more challenging. One class of problems recently arising from mobile 3D printing is the trajectory-continuous tasks, in which the end-effector is required to follow a designed continuous trajectory (time-parametrized path) in task space. This paper formulates and solves the optimal trajectory planning problem for mobile manipulators under end-effector trajectory continuity constraint, which allows considerations of other constraints and trajectory optimization. To demonstrate our method, a discrete optimal trajectory planning algorithm is proposed to solve mobile 3D printing tasks in multiple experiments.

## I. INTRODUCTION

A mobile manipulator often consists of a manipulator, such as a robotic arm, and a mobile base which helps extend the workspace of the manipulator [1], [2], [3]. This mobility feature enables the mobile manipulator to be employed in many large-scale applications which are usually considered impossible for a fixed-base robot with a similar size. The tasks for mobile manipulators can be divided into two categories: sequencing tasks and continuous tasks.

Examples of sequencing tasks are drilling [3], picking [4], inspection [5], etc. These tasks usually consist of multiple subtasks, or targets. The challenge of this class of tasks is finding the optimal sequence to perform the subtasks.

In the second category, there are path-continuous tasks and *trajectory-continuous tasks*, both of which require the mobile manipulator to perform a single continuous task. In path-continuous tasks, the end-effector must travel along a continuous path. Meanwhile, in trajectory-continuous tasks, the end-effector is required to follow a continuous trajectory (a time-parametrized path). Examples of these tasks are robotic writing [6], spraying [7], 3D printing [1], [2], etc.

In addition to finding feasible trajectories, trajectory optimization is of great importance especially in mobile manipulation. Due to the centimetre-range uncertainty of the mobile base, it is desirable to minimize an objective such as travel time or distance, effort, number of stops, etc. This problem for sequencing tasks has been solved such as by clustering the task space before task sequencing [3]. However, to the best of our knowledge, mobile base trajectory optimization has not been addressed for trajectory-continuous tasks.

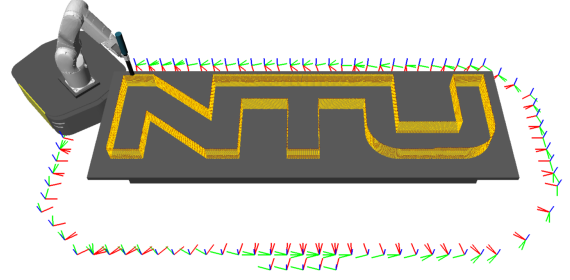


Fig. 1: Mobile 3D printing an NTU shape ( $3 \times 0.75 \times 0.15m$ ) with nozzle speed  $10cm/s$  (<https://youtu.be/yyBv3xGClnk>)

In this paper, we propose a method for planning optimal mobile manipulator trajectory in trajectory-continuous tasks, which consists in:

- Formulating the problem using configuration spacetime which reveals that this is indeed a constrained optimal trajectory planning problem subject to multiple constraints (geometric constraint, end-effector trajectory continuity and reachability, collisions, and velocity constraint) and trajectory optimization.
- Finding the optimal mobile base trajectory numerically in a discrete optimal trajectory planning algorithm.

The remainder of this paper is organized as follows. In section II, we discuss related works. Section III formulates the problem and gives an overview of some solution approaches. In section IV, we propose a discrete optimal trajectory planning method. Section V presents the applications of our method in large-scale mobile 3D printing and section VI provides some discussions.

## II. RELATED WORKS

In recent years, mobile manipulator has gained attention because of its potential in various types of tasks and brought with it challenges to motion planning. A survey can be found in [8], while technical backgrounds are explained in [9], [10].

For sequencing tasks which consist of multiple subtasks or targets between which the motion is not pre-determined, the main problem is to find the optimal sequence to visits all targets that minimizes travel time or distance, etc. This challenge has been addressed recently in [3], [4], [5], [11].

For path-continuous tasks where the robot's end-effector is required to follow a path in task space without time-parametrization, feasible base poses can be found based on reachability map [12] or inverse reachability distribution [13]. Besides, the whole-body robot motion can be controlled

<sup>1</sup>Singapore Centre for 3D Printing (SC3DP), Nanyang Technological University (NTU), Singapore [nam.ngquang@gmail.com](mailto:nam.ngquang@gmail.com)

<sup>2</sup>Eureka Robotics, Singapore

and planned online, such as using Model Predictive Control (MPC) [14], [15], [16] or Constrained Sequential Linear Quadratic Optimal Control (Constrained SLQ) [17].

Recently, from the field of large-scale mobile 3D printing for building and construction, a new class of mobile manipulator tasks has emerged which we call trajectory-continuous tasks. Compared to path-continuous tasks, these trajectory-continuous tasks require the end-effector to follow a designed trajectory (a time-parametrized path) in task space. For example, in 3D printing, the nozzle must move along the printing path at a designed speed.

To print an object larger than the reach of the manipulator, instead of using multiple robots in stationary [18], the recent trend is printing-while-moving [1]. However, most works in this field have been done with the mobile base trajectory planned manually. More recently in [2], [19], some efforts have been made in path planning for mobile manipulators based on RRT\* and inverse reachability. Limitations of this method are that it does not consider velocity constraint and only returns a jagged path which requires post-processing such as smoothing and time-parametrization [19].

In this paper, we would like to formulate the mobile manipulator motion planning problem in trajectory-continuous tasks using the configuration spacetime, which reveals that this is indeed a constrained optimal trajectory planning problem. Based on this insight, we use a light-weight, reachability guaranteed, geometric reachable region [3] to guide a discrete optimal trajectory planning algorithm in a discretized admissible base configuration spacetime which considers multiple constraints and trajectory optimization.

### III. PROBLEM FORMULATION

#### A. Configuration spacetime

The *configuration space (C-space)*  $\mathcal{C}$  is an  $n$ -dimensional manifold in which each point has  $n$  *generalized coordinates* representing the system configuration:

$$\mathbf{q} \equiv (q_1, \dots, q_n) \in \mathcal{C} \quad (1)$$

The term *spacetime* was originated from Jules Henri Poincaré in the field of Relativity, but it has also been used in Classical Mechanics [20]. Spacetime is a representation of the evolution of a dynamical system in space and time.

The term *configuration spacetime (C-spacetime)* was first used by L.P. Eisenhart (1939), A. Lichnerowicz (1955), H.D. Dombrowski and K. Horneffer (1963) [20]. Configuration spacetime  $\mathcal{X}$  is defined as the topological product of a real time axis  $\mathcal{T} \subseteq \mathbb{R}$  and the C-space:  $\mathcal{X} = \mathcal{T} \otimes \mathcal{C}$ . Thus, the configuration spacetime is an  $(n+1)$ -manifold:

$$\mathcal{X} = \{\mathbf{x} \equiv (t, \mathbf{q}) \mid t \in \mathcal{T}, \mathbf{q} \in \mathcal{C}\} \quad (2)$$

where each point  $\mathbf{x} = (t, q_1, \dots, q_n)$  is called an *event* which occurs at time  $t$  (*temporal coordinate*) when the system is having the configuration  $(q_1, \dots, q_n)$  (*spatial coordinates*).

The *trajectory* of a system is a curve  $\mathbf{q}(t)$  in C-space, or equivalently  $\mathbf{x}(s)$  in C-spacetime. In this paper, we consider  $\mathbf{q}(t)$  to be continuous, so  $\mathbf{x}(s)$  is a continuous sequence of

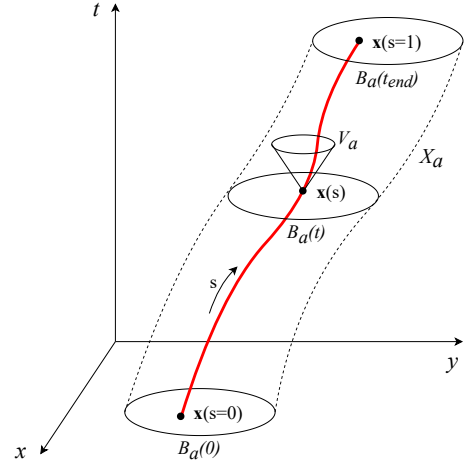


Fig. 2: Visualization of a trajectory in the base configuration spacetime (B-spacetime). The 4<sup>th</sup> dimension (orientation  $\varphi$ ) is not shown. Any point  $s \in [0, 1]$  along the trajectory must be inside an admissible B-space  $\mathcal{B}_a(t)$  and its velocity must be within a cone of admissible velocities  $\mathcal{V}_a$ . The spacetime region of admissible events (admissible B-spacetime  $\mathcal{X}_a$ ) is obtained as the admissible B-space changes in time.

events. Here, the path parameter  $s$  goes from  $s = 0$  at a start event to  $s = 1$  at an end event (see Fig. 2). The tangent vector at any point along the trajectory

$$\mathbf{x}' \equiv \frac{d\mathbf{x}}{ds} = \begin{pmatrix} t' \\ \mathbf{q}' \end{pmatrix} \quad (3)$$

must satisfy  $t' \equiv dt/ds > 0$  since time is monotonic.

The *spacetime velocity* at any point along the trajectory is parallel to the tangent vector at that point:

$$\dot{\mathbf{x}} \equiv \frac{d\mathbf{x}}{dt} = \frac{\mathbf{x}'}{t'} = \begin{pmatrix} 1 \\ \dot{\mathbf{q}} \end{pmatrix} \quad (4)$$

where  $\dot{\mathbf{q}} \equiv d\mathbf{q}/dt$  is called the *generalized velocity*.

#### B. Mobile manipulators in configuration spacetime

For example, our mobile manipulator consists of a 6-DOF manipulator  $\mathbf{q}_m = (\theta_1, \dots, \theta_6)$  and a 3-DOF planar mobile base  $\mathbf{q}_b = (x, y, \varphi)$  where  $\varphi \in \mathbb{S}^1$  is the orientation (yaw angle) of the base. Therefore, the whole-body configuration and C-space of a mobile manipulator are

$$\mathbf{q} = (\theta_1, \dots, \theta_6, x, y, \varphi) \in \mathcal{C}, \quad \mathcal{C} \subseteq \mathbb{R}^8 \otimes \mathbb{S}^1 \quad (5)$$

We follow the decoupled approach which treats the manipulator and the mobile base separately  $\mathcal{C} = \mathcal{M} \otimes \mathcal{B}$  where the *manipulator configuration space* is  $\mathcal{M} \subseteq \mathbb{R}^6$  and the *base configuration space (B-space)* is  $\mathcal{B} \subseteq \mathbb{R}^2 \otimes \mathbb{S}^1$ .

We define the *base configuration spacetime (B-spacetime)*

$$\mathbf{x} = (t, x, y, \varphi) \in \mathcal{X}, \quad \mathcal{X} \subseteq \mathbb{R}^3 \otimes \mathbb{S}^1 \quad (6)$$

where we denote  $\mathbf{x}, \mathcal{X}$  instead of  $\mathbf{x}_b, \mathcal{X}_b$  since we apply the concept of spacetime only on the mobile base, meanwhile the manipulator will be analysed using kinematic reachability.

### C. Constraints

1) *Geometric constraints*: In a 6D task, the end-effector must follow as a rigid body motion, so the task space is generally  $\mathbb{R}^3 \otimes SO(3)$ . For 5D tasks, the geometric constraints are end-effector's 3D position and 2D direction, so the task space is  $\mathbb{R}^3 \otimes \mathbb{S}^2$ . For example, 3D printing is a 5D task in which the nozzle points vertically downwards or tilts slightly from it, but the rotation around vertical axis is free. In this paper, we consider 5D tasks which bring more redundancies to the problem ( $n-5$  compared to  $n-6$ ).

2) *End-effector trajectory-continuity constraint*: The end-effector is required to follow a continuous task-space trajectory  $\mathbf{p}(t)$  instead of just a geometric path.

3) *Collisions*: The spacetime representation allows us to consider collisions between the mobile base and either static or dynamic environment by setting a safe distance from the obstacles. For a known dynamic environment, the sets of collision-free configurations of the base can be found at different times which give us  $\mathcal{B}_{free}(t) \subseteq \mathcal{B}$ . For static environment, we simply have  $\mathcal{B}_{free}(t) = \mathcal{B}_{free}(0) \forall t \in \mathcal{T}$ .

4) *End-effector reachability constraint*: For each end-effector pose in its task-space trajectory  $\mathbf{p}(t)$ , the base configuration  $\mathbf{q}_b(t)$  must be kept within an admissible set of configurations  $\mathcal{B}_a(t) \subseteq \mathcal{B}_{free}(t)$  so that the end-effector can reach the pose without violating joint limits. The set of admissible events is therefore a subset of the B-spacetime which we call *admissible B-spacetime* (see Fig. 2):

$$\mathcal{X}_a = \{\mathbf{x} = (t, \mathbf{q}_b) \mid t \in \mathcal{T}, \mathbf{q}_b \in \mathcal{B}_a(t)\} \subseteq \mathcal{X} \quad (7)$$

This set can be found based on the manipulator kinematic reachability analysis which will be discussed in section IV.B.

5) *Velocity constraint*: In this paper, we consider the (translational and rotational) velocity limits of the mobile base, so the *set of admissible spacetime velocities* is

$$\mathcal{V}_a = \{\dot{\mathbf{x}} = (1, \dot{\mathbf{q}}_b) \mid \dot{x}^2 + \dot{y}^2 \leq v_{max}^2, \dot{\phi}^2 \leq \omega_{max}^2\} \quad (8)$$

This constraint is visualized in Fig. 2: at every point on the trajectory, the spacetime velocity must be kept inside a cone.

### D. Problem formulation

The ultimate goal of mobile manipulator trajectory planning for trajectory-continuous tasks is to find the whole-body joint trajectory to perform a task without violating the constraints and optionally optimize an optimization objective.

Since finding the whole-body trajectory directly is computationally expensive, we focus on the decoupled approach which plans the trajectories for the mobile base and the manipulator separately. It is worth noting that although the whole-body planning problem is decoupled into manipulator and mobile base planning problems, they are still related: the manipulator's kinematic reachability constrains the admissible configurations of the mobile base so that the manipulator can reach the desired pose.

1) *Planning mobile base trajectory*: The *feasible trajectory planning* problem for mobile base is to find a continuous trajectory inside the admissible B-spacetime, such that the velocity at every trajectory point is an admissible velocity:

$$\mathbf{x}(s) \in \mathcal{X}_a, \quad \dot{\mathbf{x}}(s) \in \mathcal{V}_a \quad \forall s \in [0, 1] \quad (9)$$

Constraints: geometric, end-effector's trajectory-continuity and reachability constraints, and collisions, have been considered in  $\mathcal{X}_a$ ; while velocity constraint is realized by  $\mathcal{V}_a$ .

*Optimal trajectory planning*: among feasible solutions, it is desirable to find an optimal trajectory to minimize a cost:

$$\mathbf{x}^{opt}(s) = \arg \min_{\mathbf{x}(s)} J[\mathbf{x}(s)] \quad (10)$$

where  $J[\mathbf{x}(s)]$  is the cost functional, typically formulated as an integral of a Lagrangian. For example, the cost functional for minimum-effort motion is: (we denote  $a \cdot B \cdot a \equiv a^T B a$ )

$$\begin{aligned} J[\mathbf{q}_b(t)] &\equiv \int_0^{t_{end}} L(\mathbf{q}_b, \dot{\mathbf{q}}_b, t) dt = \int_0^{t_{end}} \dot{\mathbf{q}}_b \cdot \mathbf{I}_q \cdot \dot{\mathbf{q}}_b dt \\ \Leftrightarrow J[\mathbf{x}(s)] &= \int_0^1 \mathbf{x}' \cdot \mathbf{I}_x \cdot \mathbf{x}' \frac{ds}{t'}, \quad \mathbf{I}_x = \begin{pmatrix} 0 & 0 \\ 0 & \mathbf{I}_q \end{pmatrix} \end{aligned} \quad (11)$$

where the mathematical weight matrix  $\mathbf{I}_q$  is approximately proportional to the robot's inertial matrix.

2) *Manipulator trajectory planning*: Given the mobile base trajectory, the manipulator trajectory planning problem is to find an appropriate motion of the manipulator so that its end-effector follow the designed task-space trajectory.

The method of using manipulator's kinematic reachability to confine the admissible configurations of the base guarantees that IK solutions exist for finding manipulator joints for every pair of base and end-effector poses  $\mathbf{q}_b(t), \mathbf{p}(t)$ . The manipulator joint trajectory can be computed using differential IK. The rest of this paper will focus on mobile base trajectory planning.

### E. Solution approaches

A notable work recently in this area is [2]. The authors proposed a sampling-based path planning algorithm (Task-Consistent RRT\*) which then requires a post-processing phase to smooth and time-parametrize the path to get the final trajectory [19]. A possible approach is to extend this method to run in spacetime and consider velocity constraint, which will produce a trajectory instead of just a path.

We notice that the problem formulation using configuration spacetime in this section reveals an important insight: the problem is indeed constrained optimal trajectory planning instead of path planning. Since time always marches forward and the mobile base is confined inside the admissible B-spacetime, which guides the base from start to goal, the difficulty does not lie on exploring a region to find the path to goal but on constraints and optimization. Therefore, we propose a fast, complete, optimal mobile base trajectory planning algorithm based on the discrete optimal planning approach [10] in the discretized admissible B-spacetime.

#### IV. DISCRETE OPTIMAL TRAJECTORY PLANNING

##### A. Discretization

Let us sample  $N + 1$  points uniformly (in time) along the end-effector trajectory, so the corresponding mobile base trajectory consists of  $N + 1$  time steps:  $i = 0, \dots, N$ . The path parameter is  $s = i\Delta s$ ,  $\Delta s = 1/N$  and a time instance is

$$t = t_{end}s = i\Delta t, \quad \Delta t = t_{end}/N \quad (12)$$

We discretize  $\mathcal{V}_a$  by specifying a set of velocity step sizes  $\Delta v_x, \Delta v_y, \Delta \omega$  and find admissible combinations of  $(k_x, k_y, k_\phi)$  so that the admissible velocities must satisfy velocity constraint (8):  $\dot{\mathbf{x}} = (1, k_x \Delta v_x, k_y \Delta v_y, k_\phi \Delta \omega) \in \mathcal{V}_a$ . Next, we define the set of admissible controls:

$$\mathcal{U}_a = \{\mathbf{u} = \dot{\mathbf{x}}\Delta t \mid \dot{\mathbf{x}} \in \mathcal{V}_a\} \quad (13)$$

We set the step sizes of the spatial coordinates as follows:

$$\Delta x = \Delta v_x \Delta t, \quad \Delta y = \Delta v_y \Delta t, \quad \Delta \phi = \Delta \omega \Delta t \quad (14)$$

so that for any admissible controls, the mobile base at any time step  $i$  moves from one grid point to another. We use the explicit *forward Euler* discretization scheme:

$$\mathbf{x}^{i+1} - \mathbf{x}^i = \dot{\mathbf{x}}^i \Delta t = \mathbf{u}^i \quad (15)$$

where the superscripts represent different time steps.

##### B. Kinematic Reachability Analysis

We implement the kinematic reachability analysis introduced in [3]. Firstly, we discretize the space relative to the manipulator into 3D voxels of size  $\delta \times \delta \times \delta$ . Secondly, we analyse the geometry of the end-effector trajectory to specify a range of orientations. For example, in 3D printing tasks, the nozzle must be pointed downwards, and we allow  $10^\circ$  deviation from the vertical direction. Next, for each voxel position, we compute Inverse Kinematics (IK) and mark the valid voxels at which the end-effector can reach within the range of orientations determined previously. At the end of the process, a valid voxel cloud is obtained (see Fig. 3a).

From the valid voxels cloud, we determine a *geometric reachable region* for each sampling point in end-effector trajectory. This can be imagined as slicing the valid voxels cloud using: 2 horizontal planes bounding the height  $h$  of the trajectory point:  $z = h \pm \delta/2$ , 1 vertical plane  $x = X_{min}$  to keep a safe distance from the robot, and 2 spherical surfaces to close a region containing only valid voxels (see Fig. 3b).

Using the geometric reachable region with parameters  $X_{min}, Z_{min}, Z_{max}, R_{min}, R_{max}$ , the discretized admissible B-space  $\mathcal{B}_a^i$  for each end-effector pose  $\mathbf{p}(i\Delta t)$  can be obtained (see Fig. 4). Then, the discretized admissible B-spacetime is

$$\mathcal{X}_a = \bigcup_{i=0}^N \mathcal{X}_a^i, \quad \mathcal{X}_a^i = \{(i\Delta t, \mathbf{q}_b) \mid \mathbf{q}_b \in \mathcal{B}_a^i\} \quad (16)$$

In most cases, the admissible values of  $\phi$  are confined in a certain range based on the required orientation of the end-effector such as in [3]. However, in 3D printing, the nozzle axis coincides with the mobile base axis, making  $\phi \in \mathbb{S}^1$ .

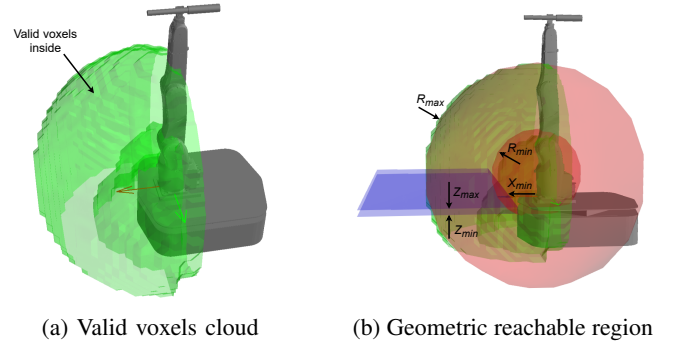


Fig. 3: Visualization of Kinematic Reachability Analysis

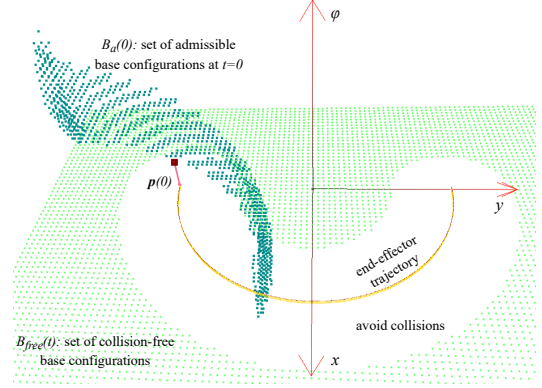


Fig. 4: Discretized admissible B-space  $\mathcal{B}_a(0)$  for end-effector pose  $\mathbf{p}(0)$ ; vertical axis shows  $\phi \in (-\pi, \pi]$  for  $\phi \in \mathbb{S}^1$

##### C. Planning optimal mobile base trajectory

We introduce the following definitions which are inspired by similar concepts in control and motion planning [21].

**Definition 1 (One-step feasible set):** The *one-step feasible set*  $\mathcal{Q}(\mathcal{I})$  is a set of admissible events  $\mathbf{x} \in \mathcal{X}_a$  that can reach at least one event  $\bar{\mathbf{x}} \in \mathcal{I}$  using one admissible control  $\mathbf{u} \in \mathcal{U}_a$ , that is  $\bar{\mathbf{x}} = f(\mathbf{x}, \mathbf{u}) = \mathbf{x} + \mathbf{u}$  (event transition equation)

$$\mathcal{Q}(\mathcal{I}) = \{\mathbf{x} \mid f(\mathbf{x}, \mathbf{u}) \in \mathcal{I}, \mathbf{x} \in \mathcal{X}_a, \mathbf{u} \in \mathcal{U}_a\} \quad (17)$$

**Definition 2 (i-stage feasible set):** The *i-stage feasible set*  $\mathcal{K}^i(\mathcal{I}^N)$  is the set of admissible events that can reach at least one event in a final set  $\mathcal{I}^N$  after a sequence of  $N - i$  admissible controls. This set can be computed iteratively by

$$\begin{aligned} \mathcal{K}^N(\mathcal{I}^N) &= \mathcal{I}^N \cap \mathcal{X}_a \\ \mathcal{K}^i(\mathcal{I}^N) &= \mathcal{Q}(\mathcal{K}^{i+1}(\mathcal{I}^N)) \end{aligned} \quad (18)$$

In our case, the goal set is  $\mathcal{I}_N = \mathcal{X}_a^N$  so (18) becomes

$$\begin{aligned} \mathcal{K}^N(\mathcal{X}_a^N) &= \mathcal{X}_a^N \cap \mathcal{X}_a = \mathcal{X}_a^N \\ \mathcal{K}^i(\mathcal{X}_a^N) &= \mathcal{Q}(\mathcal{K}^{i+1}(\mathcal{X}_a^N)) \subseteq \mathcal{X}_a^i \end{aligned} \quad (19)$$

which suggests a multistage graph where its stages are the same as the time steps of the trajectory  $i = 0, 1, \dots, N$ , and every node in the graph lies on a grid point of the discretized admissible B-spacetime ( $\mathcal{K}^i \subseteq \mathcal{X}_a^i$ ).

From (11), the numerical cost functional is:

$$J = \sum_{i=0}^{N-1} l(\mathbf{u}^i) = \sum_{i=0}^{N-1} \mathbf{u}^i \cdot \mathbf{I}_x \cdot \mathbf{u}^i \frac{1}{\Delta t} \quad (20)$$

The numerical problem is: finding the minimum-cost trajectory in a multi-source ( $\mathbf{x}^0 \in \mathcal{X}_a^0$ ) multi-goal ( $\mathbf{x}^N \in \mathcal{X}_a^N$ ) multistage graph. Instead of constructing the graph before running a graph search (such as using Dijkstra's algorithm), we propose running *backward value iterations* [10] (same as memoization in Dynamic Programming) concurrently with graph construction: while connecting the nodes using (19), concurrently calculate and store the *minimum cost-to-go*  $G(\mathbf{x})$  with the corresponding *optimal next-event*  $\bar{\mathbf{x}}^*(\mathbf{x})$  by:

$$\begin{aligned} G(\mathbf{x} \in \mathcal{K}^N) &= 0 \\ G(\mathbf{x} \in \mathcal{K}^i) &= \min_{\bar{\mathbf{x}} \in \mathcal{K}^{i+1}} \{l(\bar{\mathbf{x}} - \mathbf{x}) + G(\bar{\mathbf{x}}) \mid \bar{\mathbf{x}} - \mathbf{x} \in \mathcal{U}_a\} \\ \bar{\mathbf{x}}^*(\mathbf{x} \in \mathcal{K}^i) &= \arg \min_{\bar{\mathbf{x}} \in \mathcal{K}^{i+1}} \{l(\bar{\mathbf{x}} - \mathbf{x}) + G(\bar{\mathbf{x}}) \mid \bar{\mathbf{x}} - \mathbf{x} \in \mathcal{U}_a\} \end{aligned} \quad (21)$$

The minimum cost  $J_{\min} = \min_{\mathbf{x}} \{G(\mathbf{x} \in \mathcal{K}^0)\}$  can be found as soon as the graph is fully connected, and the memoization can be used to recover the optimal trajectory. The whole procedure is summarized in Algorithm 1 below.

---

**Algorithm 1:** Mobile base trajectory planning

---

**Input:** Discretized admissible base configuration spacetime  $\mathcal{X}_a = \{\mathcal{X}_a^0, \dots, \mathcal{X}_a^N\}$ , set of admissible controls  $\mathcal{U}_a$   
**Output:** Optimal trajectory  $\{\mathbf{x}^0, \dots, \mathbf{x}^N\}$   
1 Initialization:  $\mathcal{K}^N \leftarrow \mathcal{X}_a^N$  and  $G(\mathbf{x}) \leftarrow 0 \forall \mathbf{x} \in \mathcal{K}^N$   
/\* Backward iterations \*/  
2 **for**  $i \in [N-1, \dots, 0]$  **do**  
3    $\mathcal{K}^i \leftarrow \emptyset$   
4   **for**  $\mathbf{x} \in \mathcal{X}_a^i$  **do**  
5      $\text{ValidNode} \leftarrow \text{False}; G(\mathbf{x}) \leftarrow \infty$   
6     **for**  $\bar{\mathbf{x}} \in \mathcal{K}^{i+1}$  such that  $\bar{\mathbf{x}} - \mathbf{x} \in \mathcal{U}_a$  **do**  
7        $\text{ValidNode} \leftarrow \text{True}$   
8       **if**  $l(\bar{\mathbf{x}} - \mathbf{x}) + G(\bar{\mathbf{x}}) < G(\mathbf{x})$  **then**  
9           $G(\mathbf{x}) \leftarrow l(\bar{\mathbf{x}} - \mathbf{x}) + G(\bar{\mathbf{x}})$   
10         $\bar{\mathbf{x}}^*(\mathbf{x}) \leftarrow \bar{\mathbf{x}}$   
11       **if**  $\text{ValidNode}$  **then**  
12           $\mathcal{K}^i.\text{Insert}(\mathbf{x})$   
13   **if**  $\mathcal{K}^i = \emptyset$  **then**  
14     **return** *Infeasible*  
/\* Recover the optimal trajectory \*/  
15  $\mathbf{x}^0 \leftarrow \arg \min_{\mathbf{x}} G(\mathbf{x} \in \mathcal{K}^0)$   
16 **for**  $i \in [0, \dots, N-1]$  **do**  
17    $\mathbf{x}^{i+1} \leftarrow \bar{\mathbf{x}}^*(\mathbf{x}^i)$

---

#### D. Completeness

**Theorem 1 (Completeness):** Algorithm 1 only reports Infeasible when there is indeed no feasible trajectory.

**Proof:** Since Algorithm 1 only reports Infeasible when it runs into  $\mathcal{K}^i = \emptyset$ , we can show by contradiction that: if there exists a feasible trajectory  $\{\mathbf{x}^0, \dots, \mathbf{x}^N\}$ , then  $\mathcal{K}^i$  contains  $\mathbf{x}^i$  for all  $i \in [0, N]$ . Using backward induction:

Initialization:  $\mathbf{x}^N \in \mathcal{K}^N$  by construction.

Induction: Assume that  $\mathbf{x}^{i+1} \in \mathcal{K}^{i+1}$ ; Since  $\mathbf{x}^i$  and  $\mathbf{x}^{i+1}$  are both in a feasible trajectory, they satisfy  $\mathbf{x}^{i+1} - \mathbf{x}^i \in \mathcal{U}_a$ , which means  $\mathbf{x}^i \in \mathcal{Q}(\mathcal{K}^{i+1}) = \mathcal{K}^i$  according to (17) and (19).

#### E. Optimality

**Theorem 2 (Optimality):** If Algorithm 1 returns an output trajectory, then it is indeed the optimal trajectory.

**Proof:** Firstly, if Algorithm 1 returns a sequence  $\{\mathbf{x}^0, \dots, \mathbf{x}^N\}$ , one can show by forward induction that this sequence is a feasible trajectory.

Secondly, Algorithm 1 tracks the minimum cost-to-go and optimal steps from every node to the goal stage in the same way as dynamic programming. Therefore, by the principle of optimality [10], Algorithm 1 returns the trajectory with minimum cost-to-go from stage 0 to N, which is equivalent to the optimal trajectory with minimum cost functional.

## V. EXPERIMENTS

Our mobile manipulator consists of a DENSO VS-087 6-DOF arm mounted on a Clearpath Ridgeback 3-DOF omnidirectional mobile base. The following experiments illustrate our method in 3D printing with increasing difficulty levels. A hardware demo and a simulation example are shown in the accompanying video (<https://youtu.be/yyBv3xGClnk>).

### A. Experiment 1: Mobile 1D printing

Figure 5 shows the optimal mobile base trajectory solutions for 3 cases of mobile base in printing a horizontal line. Since the B-spacetime for 3D base is 4-dimensional  $(t, x, y, \phi)$ , Fig. 5c can only show the solution in task space.

### B. Experiment 2: Mobile 3D printing (hardware demo)

Figure 6 shows a real 3D printing task of a U shape (5 layers) with total printing path length of  $d = 19.85m$ . Our algorithm found an optimal mobile base trajectory in 3.8s (using  $\Delta t = 3s$ ,  $\Delta v_x = \Delta v_y = 5cm/s$ ,  $\Delta \omega = \pi/30 rad/s$ ).

### C. Experiments 3-4: Comparisons

We would like to compare our method with manual planning in [1]. Figure 7 shows our solution where the mobile base moves in a region  $55 \times 20cm$  instead of  $80 \times 10cm$ , with an average speed  $2cm/s$  which is lower than  $3.5cm/s$  in [1].

Next, we benchmark Algorithm 1 and compare it with a baseline (Dijkstra's algorithm) in the 3D printing task in Fig. 1: an NTU shape with length  $d = 112.9m$  (10 layers). Table I compares the computation time of two methods (both using  $\Delta t = 2.5s$ ,  $\Delta v_x = \Delta v_y = 5cm/s$ ,  $\Delta \omega = \pi/30 rad/s$ ). Algorithm 1 is faster by running the search during graph construction.

## VI. DISCUSSIONS

### A. Complexity analysis

1) *Complexity with respect to task length:* Table I shows that the computation time of Algorithm 1 increases linearly, since only the number of stages increases with task length  $N \propto d$ . This is a crucial property for large-scale applications.

2) *Complexity with respect to discretization step sizes:* Number of stages is  $N \propto 1/\Delta t$ ; number of nodes per stage is  $|\mathcal{X}_a^i| \propto (1/\Delta x \Delta y \Delta \phi) \propto (1/\Delta t^3 \Delta v_x \Delta v_y \Delta \omega)$ . Based on Algorithm 1, we expect its complexity to be no higher than  $O((1/\Delta t)^7 (1/\Delta v_x \Delta v_y \Delta \omega)^2)$ . Figure 8 shows in our test case that, as  $\Delta v = \Delta v_x = \Delta v_y$  and  $\Delta t$  decrease, the computation time increases polynomially with order  $O((1/\Delta v)^{3.9})$  and  $O((1/\Delta t)^{6.0})$  respectively (based on log-log analysis).

In our experiments, we use coarse step sizes, then apply linear interpolation to match with the controller's rate, so the trajectory is continuous and piecewise  $C^1$ -continuous.



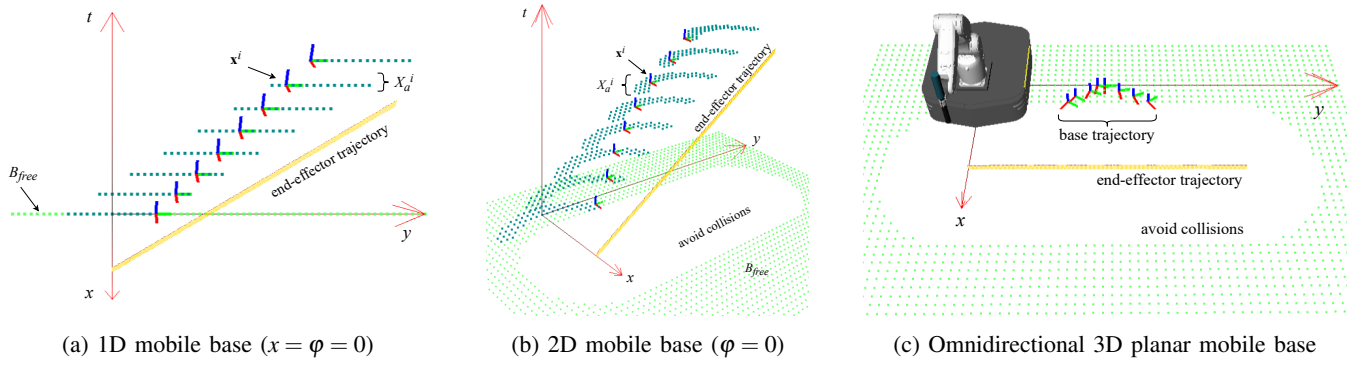


Fig. 5: Mobile 1D printing a 2.1m line with different base's DOFs. (a) and (b) are seen in B-spacetime, (c) in task space.

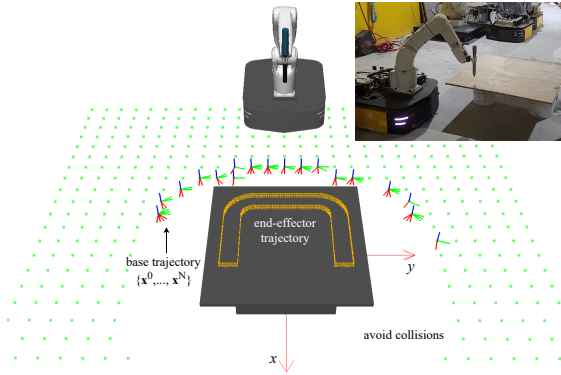


Fig. 6: Mobile 3D printing a U shape ( $0.9 \times 0.675 \times 0.05m$ ) with nozzle speed 10cm/s (<https://youtu.be/yyBv3xGClnk>)

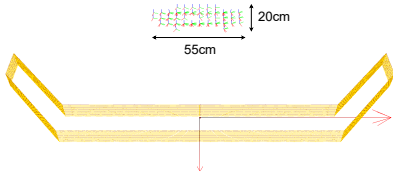


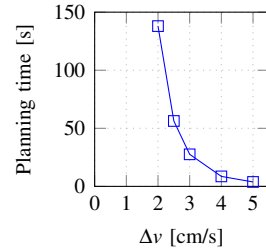
Fig. 7: Optimal base trajectory for comparison with [1]

### B. Notes on Reachability

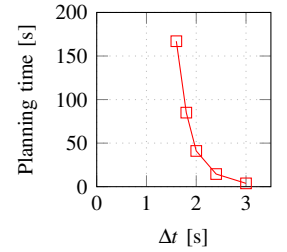
The geometric reachable region can be seen as an alternative for the inverse reachability map (IRM) [2] with some advantages. First, it is light-weight, represents the reachability using geometric parameters, hence does not require matching between IRM and the grid. In our tests, the process of finding discretized admissible B-spacetime took negligible time. Second, IK solutions exist everywhere inside the geometric reachable region, which satisfies of the manipulator reachability constraint. Although this does

TABLE I: Planning time comparison (in NTU test, Fig. 1)

Planning time for:	8 layers	10 layers	12 layers	14 layers
Algorithm 1	89.9s	108.4s	129.7s	155.1s
Baseline (Dijkstra)	120.3s	155.2s	184.4s	515.0s



(a) Planning time for 5 layers of U shape, using  $\Delta t = 3s$



(b) Planning time for 5 layers of U shape, using  $\Delta v = 5cm/s$

Fig. 8: Algorithm complexity with respect to discretization

not guarantee a continuous joint trajectory between the IK solutions [22], it is obtained in all our test cases.

### C. Notes on Kinematics

The cost functional for minimum effort in (11) effectively prevents unnecessarily large velocity changes, since a lower, stabler velocity profile has a lower effort, such as the shortest straight line in spacetime in Fig. 5a. This property makes our hardware experiment possible without post-processing. Second-order kinematic constraints such as acceleration bounds will be considered in our future works.

## VII. CONCLUSION

In this paper, we have proposed a method for formulating and solving the optimal trajectory planning for mobile manipulators under end-effector trajectory continuity constraint. We have also presented a fast, complete, and optimal algorithm to implement our method in experiments of large-scale 3D printing tasks with different levels of difficulty. Our future directions include: smoothing the mobile base trajectory, considering second-order kinematic constraints, extending to hardware motion control, and implementing sampling-based methods in our configuration spacetime formulation.

### ACKNOWLEDGMENT

This research was supported by the National Research Foundation, Prime Minister's Office, Singapore under its Medium-Sized Centre funding scheme, CES.SDC Pte Ltd, Sembcorp Architects & Engineers Pte Ltd, and Chip Eng Seng Construction Ltd.

## REFERENCES

- [1] M. E. Tiryaki, X. Zhang, and Q.-C. Pham, "Printing-while-moving: a new paradigm for large-scale robotic 3d printing," in *2019 IEEE/RSJ International Conference on Intelligent Robots and Systems (IROS)*. IEEE, 2019, pp. 2286–2291.
- [2] J. Sustarevas, D. Kanoulas, and S. Julier, "Task-consistent path planning for mobile 3d printing," in *2021 IEEE/RSJ International Conference on Intelligent Robots and Systems (IROS)*. IEEE, 2021, pp. 2143–2150.
- [3] Q.-N. Nguyen, N. Adrian, and Q.-C. Pham, "Task-space clustering for mobile manipulator task sequencing," in *2023 IEEE International Conference on Robotics and Automation (ICRA)*. IEEE, 2023, pp. 3693–3699.
- [4] J. Xu, Y. Domae, T. Ueshiba, W. Wan, and K. Harada, "Planning a minimum sequence of positions for picking parts from multiple trays using a mobile manipulator," *IEEE Access*, vol. 9, pp. 165 526–165 541, 2021.
- [5] R. Malhan and S. K. Gupta, "Finding optimal sequence of mobile manipulator placements for automated coverage planning of large complex parts," in *Proceedings of the ASME 2021 International Design Engineering Technical Conferences (IDETC)*, 2022.
- [6] K. Nagatani, T. Hirayama, A. Gofuku, and Y. Tanaka, "Motion planning for mobile manipulator with keeping manipulability," in *IEEE/RSJ international conference on intelligent robots and systems*, vol. 2. IEEE, 2002, pp. 1663–1668.
- [7] L. Pietrasik, E. Sounigo, P. Tsai, F. Gramazio, M. Kohler, E. Lloret-Fritsch, M. Hutter *et al.*, "Continuous mobile thin-layer on-site printing," *Automation in Construction*, vol. 146, 2023.
- [8] T. Sandakalum and M. H. Ang Jr, "Motion planning for mobile manipulators—a systematic review," *Machines*, vol. 10, no. 2, p. 97, 2022.
- [9] K. M. Lynch and F. C. Park, *Modern robotics*. Cambridge University Press, 2017.
- [10] S. M. LaValle, *Planning algorithms*. Cambridge university press, 2006.
- [11] F. Suárez-Ruiz, T. S. Lembono, and Q.-C. Pham, "Robotsp - a fast solution to the robotic task sequencing problem," in *2018 IEEE International Conference on Robotics and Automation (ICRA)*. IEEE, 2018, pp. 1611–1616.
- [12] F. Zacharias, C. Borst, M. Beetz, and G. Hirzinger, "Positioning mobile manipulators to perform constrained linear trajectories," in *2008 IEEE/RSJ International Conference on Intelligent Robots and Systems*. IEEE, 2008, pp. 2578–2584.
- [13] N. Vahrenkamp, T. Asfour, and R. Dillmann, "Robot placement based on reachability inversion," in *2013 IEEE International Conference on Robotics and Automation*. IEEE, 2013, pp. 1970–1975.
- [14] G. B. Avanzini, A. M. Zanchettin, and P. Rocco, "Constraint-based model predictive control for holonomic mobile manipulators," in *2015 IEEE/RSJ International Conference on Intelligent Robots and Systems (IROS)*. IEEE, 2015, pp. 1473–1479.
- [15] J.-P. Sleiman, F. Farshidian, M. V. Minniti, and M. Hutter, "A unified mpc framework for whole-body dynamic locomotion and manipulation," *IEEE Robotics and Automation Letters*, vol. 6, no. 3, pp. 4688–4695, 2021.
- [16] J. Pankert and M. Hutter, "Perceptive model predictive control for continuous mobile manipulation," *IEEE Robotics and Automation Letters*, vol. 5, no. 4, pp. 6177–6184, 2020.
- [17] M. Gifftthaler, F. Farshidian, T. Sandy, L. Stadelmann, and J. Buchli, "Efficient kinematic planning for mobile manipulators with non-holonomic constraints using optimal control," in *2017 IEEE International Conference on Robotics and Automation (ICRA)*. IEEE, 2017, pp. 3411–3417.
- [18] X. Zhang, M. Li, J. H. Lim, Y. Weng, Y. W. D. Tay, H. Pham, and Q.-C. Pham, "Large-scale 3d printing by a team of mobile robots," *Automation in Construction*, vol. 95, pp. 98–106, 2018.
- [19] J. Sustarevas, D. Kanoulas, and S. Julier, "Autonomous mobile 3d printing of large-scale trajectories," in *2022 IEEE/RSJ International Conference on Intelligent Robots and Systems (IROS)*. IEEE, 2022, pp. 6561–6568.
- [20] M. Trümper, "Lagrangian mechanics and the geometry of configuration spacetime," *Annals of Physics*, vol. 149, no. 1, pp. 203–233, 1983.
- [21] H. Pham and Q.-C. Pham, "A new approach to time-optimal path parameterization based on reachability analysis," *IEEE Transactions on Robotics*, vol. 34, no. 3, pp. 645–659, 2018.
- [22] Z. Xian, P. Lertkultanon, and Q.-C. Pham, "Closed-chain manipulation of large objects by multi-arm robotic systems," *IEEE Robotics and Automation Letters*, vol. 2, no. 4, pp. 1832–1839, 2017.